JOURNAL OF PROPULSION AND POWER
Vol. 24, No. 4, July–August 2008

Ablative Impulse Characteristics of Polyacetal with Repetitive CO_2 Laser Pulses

Koji Suzuki* and Keisuke Sawada†
Tohoku University, Sendai 980-8579, Japan
and
Ryota Takaya‡ and Akihiro Sasoh§
Nagoya University, Nagaya 464-8603, Japan

DOI: 10.2514/1.32477

Impulse characteristics for a polyacetal target repetitively irradiated with pulses from a transversely excited atmospheric CO_2 laser were experimentally investigated. About 10-J laser pulses were repetitively irradiated up to 110 times onto a 6.6- or 8.6-mm-diam spot on the target, which was mounted on a torsion-type impulse balance. In the first several laser pulses, the impulse and ablation rate were strongly influenced by the initial conditions of the target surface. After ten cleaning pulses, 100 pulses were irradiated in various burst modes. Successive laser pulses in a burst were irradiated at a repetition frequency of 50 Hz. The time interval between successive bursts was greater than 3 min. The momentum coupling coefficient C_m was almost independent of the burst mode. With a fluence of 18.8 J/cm^2, C_m gradually increased with an increasing total number of pulses, reaching 220 μN · s/J at an ambient pressure of 10^{-2} Pa and 145 μN · s/J in the atmosphere. When the fluence was 31.8 J/cm^2, C_m began to decrease after about 50 pulses. C_m was smaller for a smaller spot diameter. Those impulse characteristics were closely associated with target surface morphology and fluid dynamics of the ablation plume and the ambient air.

Nomenclature

C	=	dumping constant
C_m	=	momentum coupling coefficient
d	=	laser spot diameter
E	=	laser energy
f	=	focal length
g	=	function, Eq. (6); gravitational acceleration, Eqs. (14) and (15)
i	=	serial number of laser pulse
I_m	=	constant value of impulse
$\bar{I}_m(N)$	=	total impulse integrated up to *Nth* laser pulse
$I_{m,i}$	=	impulse induced by *i*th laser pulse
J	=	angular moment of inertia
K	=	spring constant
m	=	ablator mass
N	=	total number of laser pulses
P_0	=	ambient pressure
r_D	=	radial location of displacement sensor
r_L	=	radial location of laser pulse irradiation
t	=	time, originated in (first) laser pulse initiation
u	=	step function
α	=	ablation rate
ΔN	=	number of laser pulses in a burst
$\Delta\tau_L$	=	time interval between successive laser pulses
δ	=	Dirac delta function
θ	=	deflection angle
ϕ	=	fluence
τ_B	=	natural oscillation period of impulse balance
τ_L	=	total period of laser pulse irradiations

Presented as Paper 4389 at the 38th AIAA Plasmadynamics and Lasers Conference, Miami, FL, 25–28 June 2007; received 29 May 2007; revision received 1 April 2008; accepted for publication 3 April 2008.

*Graduate Student, Department of Aerospace Engineering; currently Ishikawajima-Harima Heavy Industries Company, Ltd., 3-1-1 Toyosu, Koto-ku, Tokyo 135-8710, Japan.

†Professor, Department of Aerospace Engineering, 6-6-2 Aramaki-Aza-Aoba. Associate Fellow AIAA.

‡Graduate Student, Department of Aerospace Engineering, Furo-cho, Chikusa-ku.

§Professor, Department of Aerospace Engineering, Furo-cho, Chikusa-ku. Associate Fellow AIAA.

I. Introduction

LASER propulsion [1] is one of the most promising methods of remotely generating an impulse without carrying a power supply onboard. Using a solid propellant and laser ablation, a propellant storage tank is not necessary. In operation in the atmosphere, an impulse that is generated only through gaseous breakdown can be enhanced by ablative momentum flux [2,3].

The ablative impulse characteristics induced by a single laser pulse have been reported for various types of lasers, targets, and ambient-air conditions [4–21]. Gregg and Thomas [4] measured the impulse caused by irradiating metals with ruby laser pulses and concluded that the momentum coupling coefficient C_m, which is the ratio of laser-induced impulse to laser energy, has a maximum with respect to laser intensity. Phipps et al. [5] proposed formulas for a laser-ablative impulse by integrating experimental and theoretical data on metals and polymers. They also supported the aforementioned laser intensity dependence of C_m. Pakhomov et al. [8,9] investigated laser-impulse characteristics of various metals; they also highlighted the effect of ambient-air pressure on the impulse [10,11]. Watanabe et al. [14] determined an optimum condition with respect to both the laser fluence and the ambient pressure when irradiating a target made of polyacetal (POM) with a transversely excited atmospheric (TEA) CO_2 laser pulse. This combination of laser and polymer gave the most favorable impulse performance among the polymers tested.

The existence of an optimum fluence implies that to optimize propulsion performance, irradiating with a giant pulse of excessively high fluence should be avoided. If the laser irradiation area on a target is not large enough, C_m can be maximized by repetitively irradiating laser pulses with the energy corresponding to the optimum fluence. If the total impulse increases linearly with the number of laser pulses of a constant energy, we can develop a high-performance propulsion device. The same principle applies to laser-powered space debris deorbiting [22].

Phipps et al. [23] developed a laser plasma thruster, in which repetitive laser pulses were irradiated onto successive virgin spots on a sliding propellant tape. Other physicochemical effects such as etching rate, [24] ablation threshold, [25] transmission coefficient, [26] and surface morphology [27], etc., of repetitively irradiated laser pulses on polymers have been investigated and reported. However, the impulse characteristics of repetitively irradiating laser pulses onto a fixed spot have not been well reported, at least in the open literature. The purpose of this study is to experimentally investigate the impulse characteristics of POM to repetitive TEA CO_2 laser pulses irradiated onto a fixed spot, as well as to understand associated physical mechanisms.

II. Apparatus and Methods

A. Design of Impulse Balance

Figure 1 shows the schematic diagram of the impulse balance developed in this study. This is a torsion-type balance [16] that has a 1-m-long, horizontally set, main arm made of aluminum. The arm is supported by two pivots on the upper and lower surfaces at the center of the arm. The sensitivity and natural oscillation period τ_B can be controlled by the radial location of the symmetrically set, 9-kg weights (W1 and W2). With these weights being set at the edges of the arm, τ_B can be as long as about 30 s. To increase the sensitivity of the balance, measurement without the weights is also possible. Fine static balance adjustment was accomplished using the other weights (W3 and W4). An ablative impulse is exerted at $r = r_L$. The deflection of the arm is measured at $r = r_D$ using an eddy-current linear displacement sensor. A calibrated impulse is exerted using a ballistic hammer with a piezoelectric force sensor (208C1, PCB, Inc., sensitivity of 112.4 m V/N and force range of ±44.5 N). Active damping was done with the electromagnet.

In this study, an impulse induced by a single laser pulse is completed within 10 μs [21,28], whereas the period of the natural frequency is more than 10^6 times longer. An impulse that is induced by a single laser pulse can be modeled using the Dirac delta function. The equation of motion of the balance yields

$$J\frac{\mathrm{d}^2\theta}{\mathrm{d}t^2} + C\frac{\mathrm{d}\theta}{\mathrm{d}t} + K\theta = r_L\sum_{i=1}^{N} I_{m,i}\delta(t-(i-1)\Delta\tau_L) \tag{1}$$

The solution of Eq. (1) for $\theta(0) = \mathrm{d}\theta(0)/\mathrm{d}t = 0$ and $C = 0$ is

$$\theta(t) = \frac{r_L}{\sqrt{JK}}\sum_{i=1}^{N} I_{m,i}\sin\left\{\sqrt{\frac{K}{J}}(t-(i-1)\Delta\tau_L)\right\}\cdot u(t-(i-1)\Delta\tau_L) \tag{2}$$

The maximum deflection angle induced by a single laser pulse can be obtained by substituting $N = 1$ into Eq. (2):

$$\theta_{\max}(1) = \frac{r_L I_m}{\sqrt{JK}} \tag{3}$$

where $I_m = I_{m,1}$.

The maximum deflection angle as a result of N-impulse exertions with a constant time interval of τ_L is obtained from Eq. (2):

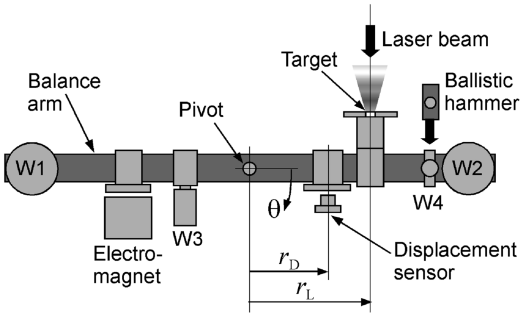

Fig. 1 Top view of the schematic of impulse balance.

$$\theta_{\max}(N) = \frac{r_L}{\sqrt{JK}}\sum_{i=1}^{N} I_{m,i}\cos\left\{\sqrt{\frac{K}{J}}\left(\frac{N-1}{2}-i+1\right)\Delta\tau_L\right\} \tag{4}$$

If $I_{m,i}$ has a constant value of I_m, Eqs. (3) and (4) yield

$$\theta_{\max}(N) = \theta_{\max}(1)g\left(\frac{\tau_L}{\tau_B}\right) \tag{5}$$

$$g\left(\frac{\tau_L}{\tau_B}\right) \equiv \sum_{i=1}^{N}\cos\left\{\pi\left(1-\frac{2(i-1)}{N-1}\right)\frac{\tau_L}{\tau_B}\right\} \tag{6}$$

$$\tau_L \equiv (N-1)\Delta\tau_L \tag{7}$$

$$\tau_B \equiv 2\pi\sqrt{\frac{J}{K}} \tag{8}$$

As shown in Fig. 2, g is a decreasing function of τ_L/τ_B that equals unity only when τ_L and then $\Delta\tau_L$ vanish. The condition to allow a 1% error (that is, $g \geq 0.99$) is given by

$$\frac{\tau_L}{\tau_B} \leq 0.078 \tag{9}$$

In this study, the design criterion of Eq. (9) was employed; to obtain 99% accuracy for the total impulse from 100 3-mNs impulses with a repetition frequency of 50 Hz for 2 s, τ_B should be longer than 25.6 s. The control parameters involved in the balance design are J, K, r_L, and r_D. Their values were determined from the following conditions: 1) allowable load to the pivots, 2) maximum deflection at $r = r_D$, 3) allowable error with respect to the laser spot location, and 4) allowable error in fluence caused by the swing of the arm. The value of $\theta_{\max}$ was converted to the maximum linear deflection measured at $r = r_D$. The design specifications were $J = 4.01$ kgm^2, $K = 0.192$ Nm/rad, $r_L = 0.100$ m, and $r_D =$ 0.100 m, respectively, to yield a maximum impulse of 438 mNs with a resolution of 0.175 mNs, and $t_B = 28.7$ s for the maximum linear deflection of ±5.0 mm. The impulse-deflection relation was fit to a quadratic equation in the calibration before and after every series of experiments of the day.

B. Apparatus

Figure 3 shows the schematic diagram of the experimental setup. TEA CO_2 laser (wavelength of 10.6 mml, SLCR-Lasertechnik GmbH, ML205) [28] pulses were introduced to the vacuum chamber (inner diameter of 0.7 m and length of 2.0 m) after being reflected from two collimating molybdenum mirrors and sent through a ZnSe plane-convex lens of a focal length of 1.07 m. The laser beam has a diameter of 55 mm at the oscillator exit. The energy of a single laser pulse was measured with an energy meter (ED-500LIR, Gentec

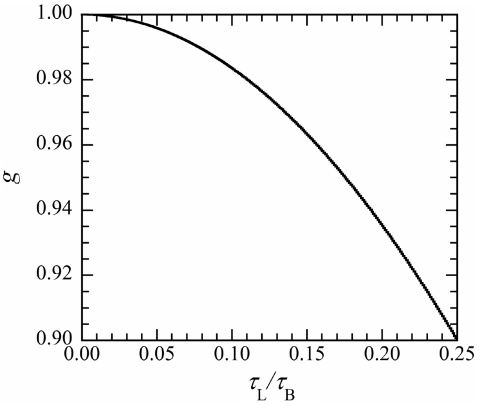

Fig. 2 Gain to multiple impulses of constant magnitude exerted at a constant repetition frequency.

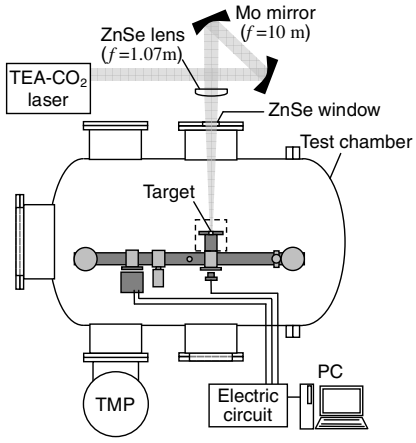

a)

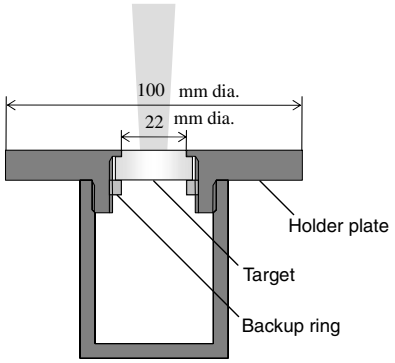

b)

Fig. 3 Experimental setup: a) whole, b) close-up near the target.

Electro-Optics, Inc.); time variation of the intensity was measured with a photon-drag sensor (B749, Hamamatsu Photonics). The laser pulse had a primary peak intensity of 60 MW/cm^2 for a total energy of 10 J, full width at half-maximum of 170 ns with 90% of the total energy output within 3.1 μs.

The impulse balance was set in the vacuum chamber with its arm parallel to the chamber axis. As shown in Fig. 3b, the target was placed in the holder, which in turn was attached to the side face of the balance arm. The target was made of ployacetal (POM), 10 mm in thickness and 22 mm in diameter on the incident surface, flush-mounted on a 100-mm-diam aluminum holder plate. The laser beam was irradiated normal to the target surface. Before laser pulse irradiance, the target surface was not mechanically or chemically processed, only cleaned using ethanol. The vacuum chamber was evacuated using a turbomolecular pump (TMP-2003LM, Shimazu, 2000 liter/s for N_2), which in turn was backed by a rotary pump (T2033SD, Alcatel, 500 liter/min). The pumps were kept in operation even during laser pulse irradiations.

III. Results and Discussions

According to Watanabe et al. [14], the highest C_m was obtained for a fluence of 18 J/cm^2. In their experiments, a laser pulse was irradiated onto a 30 × 30 mm square on the target surface, whereas in this study, the laser spot has a smaller dimension: that is, a circle of 8.6 mm or less in diameter. Because the laser pulse durations were of the same order, the edge effect (that is, the effect of expansion waves from the peripheral of the laser spot) was larger in this experiment. Although the optimum fluence can be quantitatively different due to this scaling effect, the preceding value is regarded as a good reference. Therefore, in this study, we set a fluence of 18.8 J/cm^2 as the nominal operation condition. This corresponded to a laser energy of 10.9 J and a spot diameter of 8.6 mm. The ambient-air pressure P_0 was set either to 10^{-2} or to 10^5 Pa. Laser pulses were irradiated in burst mode. In a burst, laser pulses of a constant energy were irradiated onto the target at a repetition frequency of 50 Hz. The time interval between successive bursts was set to longer than 3 min. The impulse measurement was continued up to 110 laser pulses without changing the target and optics arrangements.

Here, let N and ΔN designate the accumulated number of laser pulses and the number of laser pulses in a burst, respectively. C_m and the ablation mass reduction rate, which hereafter will be referred to as the *ablation rate* α, are defined as follows:

$$C_m(N - \Delta N/2) = \frac{1}{E\Delta N}\{\bar{I}_m(N) - \bar{I}_m(N - \Delta N)\} \tag{10}$$

$$\bar{I}_m(N) = \sum_{i=1}^{N} I_{m,i} \tag{11}$$

$$\alpha_{N-\Delta N/2} = \left|\frac{m(N) - m(N - \Delta N)}{E\Delta N}\right| \tag{12}$$

When measuring the impulse induced by a single laser pulse ($\Delta N = 1$), the balance sensitivity was increased by removing W1 and W2 (Fig. 1) from the balance arm. The impulse generated in a burst of $\Delta N \geq 10$ was measured in the balance arrangement shown in Fig. 1. Because the mass reduction was sensitive to the location and orientation of the laser spot, the ablation rate was measured only once for each target. The differentiation in Eq. (12) was obtained by collecting the mass reduction data of three to five different targets for each N. Because the test chamber is large enough (with an inner diameter of 0.7 m and a length of 2 m), the surface area ratio of the target to the test chamber was 7×10^{-5}. The mass fraction of redeposition was even smaller because we continued to run the vacuum pumps even during the test period. Therefore, we neglected the redeposited mass in the evaluation of Eq. (12).

A. Nominal Fluence (18.8 J/cm^2), $N \leq 10$

As will be described in detail later, because in initial several shots the impulse exhibited considerably different characteristics from later shots, we treated the first ten shots against a virgin target as cleaning shots. In this subsection, impulse characteristics in the cleaning shots will be described. Figure 4a shows the variations of C_m as a function of $N(\leq 10)$ measured for $\Delta N = 1$ with $\phi = 18.8$ J/cm^2. For both of the ambient pressures, P_0, C_m started at a relatively low value: 88 μN · s/J for $P_0 = 10^5$ Pa and 140 μN · s/J for $P_0 = 10^{-2}$ Pa, respectively. The respective levels increased: 192 ± 8 μN · s/J in the second pulse and thereafter for $P_0 = 10^{-2}$ Pa and 117 ± 7 μN · s/J in the fifth and thereafter for $P_0 = 10^5$ Pa. The initial variations of the ablation rate shown in Fig. 4b were also large. For $P_0 = 10^5$ Pa, the ablation rate started as low as 70 μg/J, then increased to 170 μg/J with a scatter of ± 30 μg/J. For $P_0 = 10^{-2}$ Pa, the ablation rate was 185 μg/J in the first pulse, then settled down to the same level as in the former. Figure 5 shows open-shutter pictures of radiating ablation plumes. For $P_0 = 10^{-2}$ Pa, a radiating violet flare plume was clearly observed only in the first shot. For $P_0 = 10^5$ Pa, the plume became somewhat spherical and orange-colored and could be observed up to the fourth shot; after that, it was observed only sporadically. Therefore, the observed radiation from the ablation plume almost corresponded to the aforementioned impulse and ablation rate characteristics; when the radiating plume appeared, the impulse was small. We also conducted Langmuir probe measurements. However, signals were obtained only for $P_0 = 10^{-2}$ Pa and when such a radiating plume was observed.

Figure 6 shows framing schlieren images of a laser ablation plume and associated flows for $P_0 = 10^5$ Pa. In the case of $N = 1$ (Fig. 6a), a laser-induced plasma appeared in frame 1 as a radiating zone on the target surface. The plasma expanded in an almost-hemispherical shape. In frame 4 and thereafter, a hemispherical shock wave was observed as a detached density discontinuity ahead of the contact surface of the plasma. Along the center axis, the frontal portion of the

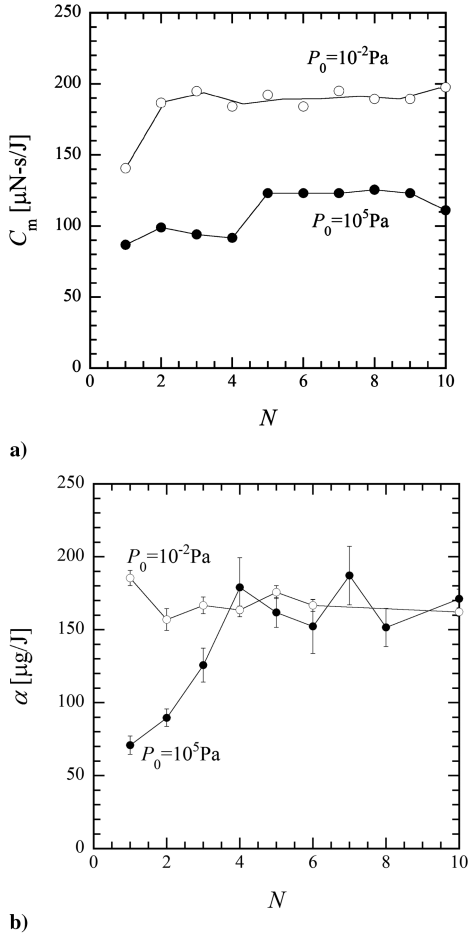

Fig. 4 Variations of C_m and α as a function of N ($N \leq 10$); $\Delta N = 1$, $E = 10.9$ J, and $d = 8.6$ mm ($\phi = 18.8$ J/cm^2).

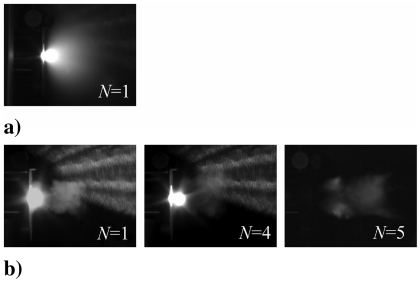

Fig. 5 Open-shutter photographs of ablation plume: a) $P_0 = 10^{-2}$ Pa and b) $P_0 = 10^5$ Pa [fringes in the upper-right portion of the images ($N = 1$ and 4) are a reflection from the chamber inner wall]; $E = 10.9$ J, $d = 8.6$ mm ($\phi = 18.8$ J/cm^2), and $\Delta N = 1$.

plasma continued to emit radiation up to frame 5. This zone shields the target surface against the laser power, thereby lowering the pressure on it. These results are consistent with the Anju et al. [28] results obtained using a velocity interferometer. Because the laser power was partially absorbed ahead of the target surface, the solid angle of the almost-hemispherical shock wave was larger than 2 τ_L. In the case of $N = 3$ (Fig. 6b), the radiation from the plasma [5] became weaker. As will be shown later for $N > 10$, the radiating zone was observed only sporadically. This implies that in the first several shots, the zone of laser power absorption detached from the target surface, and so the energy transfer to the ablative impulse generation was decreased. This is no less than the plasma shielding effect and is consistent with the aforementioned impulse and mass consumption performance.

Figure 7 shows framing schlieren images for $P_0 = 10^{-2}$ Pa and $N = 1$. A radiating zone was observed in frame 1 only for $N = 1$. In a

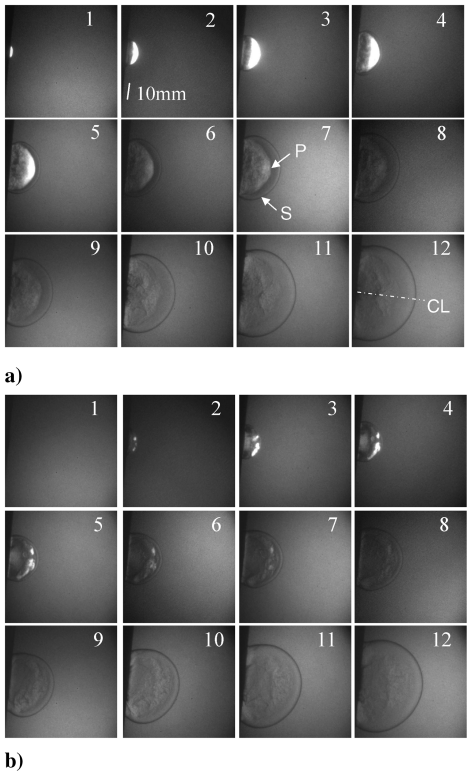

Fig. 6 Framing schlieren images: a) $N = 1$ and b) $N = 3$; $E = 10.9$ J, $d = 8.6$ mm ($\phi = 18.8$ J/cm^2), $P_0 = 10^5$ Pa, exposure time is 0.1 μs, framing rates are 1 μs (frames 1–8) and 2 μs (frames 9–12); P denotes plasma, S denotes shock wave, and CL denotes the centerline.

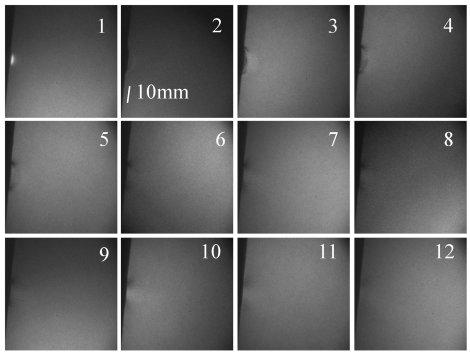

Fig. 7 Framing schlieren images; $E = 10.9$ J, $d = 8.60$ mm ($\phi = 18.8$ J/cm^2), $P_0 = 10^{-2}$ Pa, $N = 1$, exposure time is 0.1 μs, and framing rates are 0.5 μs (frames 1–8) and 1 μs (frames 9–12).

separate series of experiments, we conducted diagnostics using Langmuir probes (single and triple probes). However, at this fluence, the probe signal was obtained only in the first shot. The C_m and ablation rate characteristics special to the first shot (Fig. 4) should have a close link to this radiating zone. Although, due to the low-density level, the contrast in those frames is poorer, an ablation plume was observed in frame 7 and later. The diameter of the plume was almost equal to d. There will be further discussion on this issue in the next subsection.

Figure 8 shows scanning electron microscope images of the target surface. Figure 8a shows the whole area of the laser irradiated spot for $N = 10$. Regions A, B, and C are the central, periphery, and outside of the laser spot, respectively. The broken line is the effective boundary of the laser spot. In region A, fringes on the order of 300 μm that corresponded to the laser beam pattern are observed. Figures 8b and 8c compare region A before ($N = 0$) and after ($N = 5$) laser pulse irradiations, respectively. As shown as region C in Fig. 8a, (spatial resolution of 100 μm) the initial surface looks

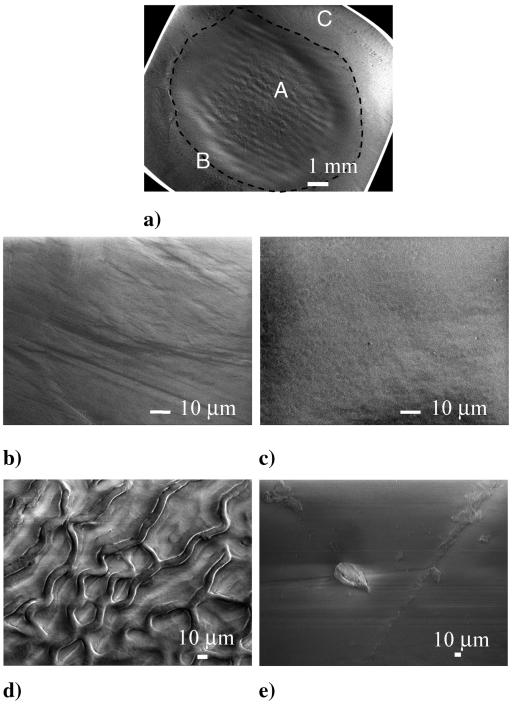

Fig. 8 Scanning electron microscope images of the laser spot: a) whole spot, $N = 10$, b) region A, $N = 0$ (initial surface), c) region A, $N = 5$, d) region B, $N = 10$, e) region C, $N = 1$; $P_0 = 10^5$ Pa, $E = 10.9$ J, $d = 8.6$ mm ($\phi = 18.8$ J/cm^2), and $\Delta N = 1$.

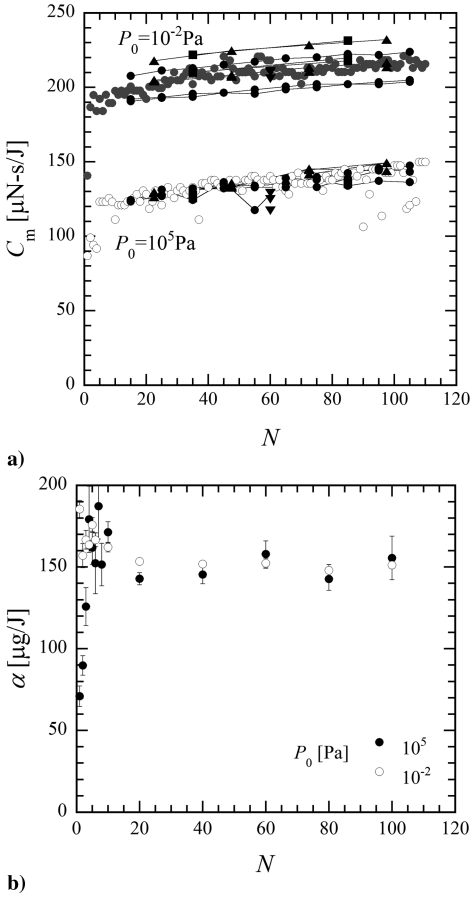

Fig. 9 Variations of C_m and α as a function of N ($N \leq 110$): a) $\Delta N = 1$ and $P_0 = 10^{-2}$ Pa (gray circles), $\Delta N = 1$ and $P_0 = 10^5$ Pa (open circles), $\Delta N = 10$ (black circles), $\Delta N = 25$ (upward triangles), $\Delta N = 50$ (squares), and $\Delta N = 100$ (downward triangles) and b) $\Delta N = 1$, $E = 10.9$ J, and $d = 8.6$ mm ($\phi = 18.8$ J/cm^2).

smooth. However, with finer scale it shows grooves that are several microns thick, as seen in Fig. 8b. Those grooves were smoothed out after five laser pulses (Fig. 8c). In region B (Fig. 8d), filament structures appeared. The formation of a similar structure was assumed to be due to a fluid dynamic processes in which the melt became solidified [29]. This structure appeared both at $P_0 = 10^5$ and 10^{-2} Pa. Figure 8e shows an example of debris appearing after irradiating with a single laser pulse. Such debris, with dimensions of several tens of microns, appeared only for $P_0 = 10^5$ Pa. For $P_0 = 10^{-2}$ Pa, only submicron-order particles were deposited in region C.

In the Watanabe et al. [14] free-flight experiments, and many other experiments, the impulse performance and mass consumption were measured only with a virgin specimen, corresponding to an $N = 1$ shot in this study. The initial C_m and ablation rate characteristics roughly reflect the multiple-pulse performance, yet quantitatively did not agree. As will be presented in detail later, in each laser pulse, on average, a layer with thickness of about 40 μm was removed due to ablation. There must be a chemical or thermal surface layer with a thickness of this order. Moreover, as seen in Fig. 8, the surface condition changed even on the millimeter scale. As a result, the impulse and ablation characteristics of the virgin surface exhibited complicated behaviors (see Fig. 4). Yet, in evaluating the impulse performance over a large number of laser pulses, such initial behaviors become less and less important by increasing the number of pulses. Therefore, in each experiment, the first ten laser pulses were applied as cleaning shots over an interval of greater than 3 min. The impulse characteristics in the subsequent 100 shots were primarily highlighted.

B. Nominal Fluence (18.8 J/cm^2), $10 < N < 110$

After the cleaning shots (that is, for $N > 10$), laser pulses were irradiated in burst mode. In a burst, laser pulses of a constant energy of 10.9 J were irradiated at a constant repetition frequency of 50 Hz. The number of laser pulses in a burst, ΔN, was set either to 1, 10, 25, 50, or 100. The interval between successive bursts was set longer than 3 min. The total number of laser pulses was set to 110.

Figure 9a shows the variations of C_m measured for the nominal fluence. In this figure and hereafter, the symbols are plotted at the local-average values according to Eqs. (10) and (12). N includes the first ten pulses of cleaning shots. As was obtained for $N < 10$ in the previous section, a higher level of C_m was obtained for $P_0 = 10^{-2}$ Pa than for $P_0 = 10^5$ Pa. Usually, the laser-induced impulse decreases by decreasing the ambient pressure [3,10,30]. In [3], C_m with Derlin (a POM homopolymer) against a CO_2 laser pulse (duration of 12 μs) measured for fluences of higher than 165 J/cm^2 monotonically decreased by decreasing the ambient pressure. However, according to Watanabe et al. [14], C_m with fluence of 18 J/cm^2 became higher at the reduced pressure. The condition of Fig. 9 is back to the latter case, thereby quantitatively agreeing with [14,28]. (It should be noted here that in [14,28] the impulse characteristics were measured only with the virgin target.) The C_m level was much increased in the later shots. For $P_0 = 10^5$ Pa, C_m exceeded 120 μN $\cdot$ s/J in most of the later shots for $N > 10$, whereas it was lower than 100 μN $\cdot$ s/J for $N < 5$. For $P_0 = 10^{-2}$ Pa, C_m was greater than 190 μN $\cdot$ s/J for $N > 10$, whereas it was 140 μN $\cdot$ s/J only at $N = 1$. As seen in Fig. 9a, for $P_0 = 10^5$ Pa even for $N > 10$, C_m sporadically dropped from its average value by up to 25%. Only in such shots did we observe a strong radiation emission near the target surface, as shown in Fig. 5; the air breakdown caused by contaminants in the ambient air occurred occasionally. In the case of $P_0 = 10^{-2}$ Pa, such breakdown did not occur for $N > 1$.

In the measured C_m performance in the $10 \leq N \leq 110$ range, the influence of ΔN did not clearly appear, except for the case of $\Delta N = 100$ for $P_0 = 10^5$ Pa, in which the ablated gas was presumably not fully evacuated, because the vacuum chamber has a finite volume. At least at that low repetition frequency of 50 Hz, the effects of target preheating and residual gas over the target did not affect the impulse performance as long as the pumping capability of the vacuum chamber was sufficiently high.

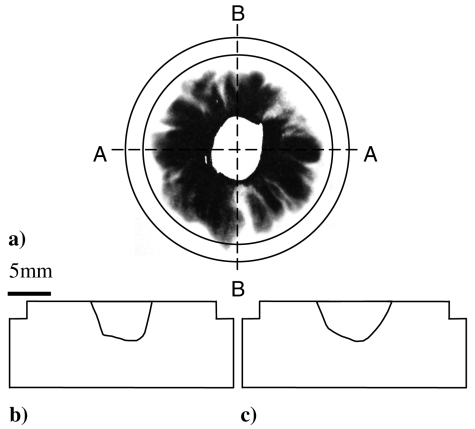

Fig. 10 Sketch of crater: a) front view (laser energy distribution recorded on photosensitive paper), b) cross section A–A, and c) cross section B–B; $N = 110$, $P_0 = 10^5$ Pa, $E = 10.9$ J, $d = 8.6$ mm ($\phi = 18.8$ J/cm^2), and $\Delta N = 1$.

In the $10 \leq N \leq 110$ range for $P_0 = 10^5$ Pa, C_m started at 124 μN · s/J ($N = 15$) and increased by 15%. For $P_0 = 10^{-2}$ Pa, C_m increased by 8% from 200 μN · s/J ($N = 15$). These increases in C_m should be closely related to the formation of craters. Figure 10 shows the sketches of the crater that was formed at $N = 110$ for $P_0 = 10^5$ Pa. In Fig. 10a, a laser beam pattern recorded onto a photosensitive paper sheet is superimposed on the target outline. The white portion at the center is the region where most of the laser energy was irradiated. Figures 10b and 10c are cross-sectional views of the crater. The crater is in the rough shape of a truncated ellipsoid. On the target surface, its major and minor axes are approximately 9 and 7 mm, respectively. From the volume measured in these sketches, the ablated mass rate and surface receding rate are estimated to be 170 ± 30 μg/J and 40 ± 5 μm/pulse, respectively. Within the experimental uncertainty, these values agree with the experimentally measured ablation rate shown in Fig. 9b. As seen in Fig. 9b, the ablation rate became almost constant at $150 \pm 20 \mu$g/J and did not depend on P_0.

The most possible effect of crater formation on the impulse is jet formation. For $P_0 = 10^5$ Pa in the case of $N = 1$ (Fig. 6a), the contact surface retained its spherical shape. However, a flare structure of the ablation jet appeared even for $N = 3$ (Fig. 6b). In the $N = 20$ shot shown in Fig. 11a, the flare structure was even enhanced (see frames 10 to 12); being driven by the ablation plume, the hemispherical shock wave extruded forward along the axis. In the case of $N = 100$ (Fig. 11b), the eccentricity of the shock wave increased. At this stage, the crater was formed, as shown in Fig. 10. The crater acted as an aerodynamic nozzle, enhancing the axial momentum flux of the plume and thus the impulse performance. Because the crater surface had a few-millimeter-order irregularities, the contact surface of the plume became much more disturbed.

For $P_0 = 10^{-2}$ Pa, the processes of ablation-plume concentration were clearly observed, as shown in Fig. 12. With increasing N, the diameter of the ablation plume decreased; the effective plume diameter varied from 8 mm ($N = 1$) to 5 mm ($N = 100$). With the growth of the crater depth, the ablation plume gained better directionality to the axis, thereby increasing the momentum in the axial direction and the pressure on the ablator surface. As a result, a similar impulse enhancement to that for $P_0 = 10^5$ Pa was also obtained (see Fig. 9a).

Due to the limited space available for the visualization setup, in all of the images in Figs. 6, 7, 11, and 12, the laser axis normal to the target is inclined by 5.5 deg from the horizontal [see frame 12 in Fig. 6a].

C. High Fluence (31.8 J/cm^2)

Figures 13 and 14 show C_m variations and the sketch of the crater when the fluence was 31.8 J/cm^2 for $P_0 = 10^{-2}$ Pa. As occurred with the nominal fluence in Fig. 9a, C_m did not depend on ΔN, except

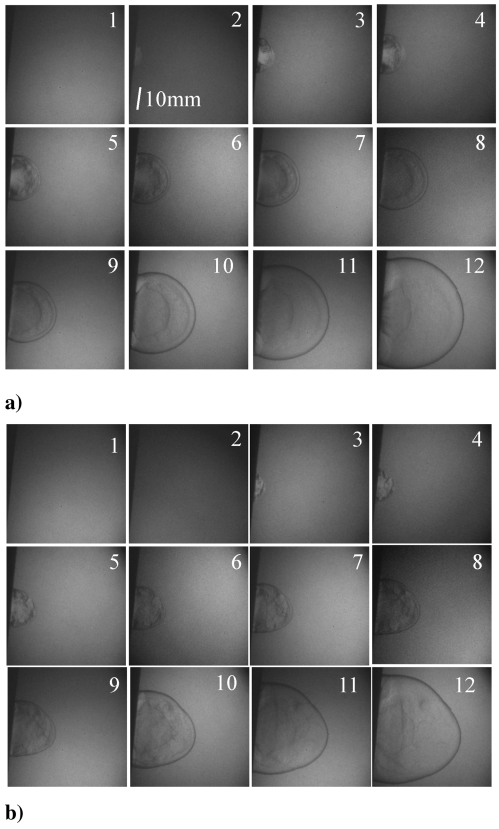

Fig. 11 Framing schlieren images: a) $N = 20$–22 and b) $N = 100$–102; $E = 10.9$ J, $d = 8.6$ mm ($\phi = 18.8$ J/cm^2), $P_0 = 10^5$ Pa, exposure time is 0.1 μs, and framing rates are 1 μs (frames 1–8) and 4 μs (frames 9–12).

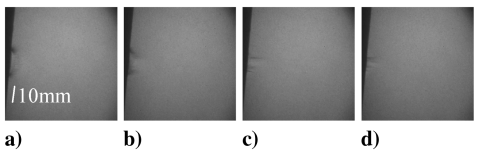

Fig. 12 Framing schlieren images: a) $N = 1$, b) $N = 20$, c) $N = 60$, and d) $N = 100$; $E = 10.9$ J, $d = 8.6$ mm ($\phi = 18.8$ J/cm^2), $P_0 = 10^{-2}$ Pa, $t = 2.0$ μs, and exposure time is 0.1 μs.

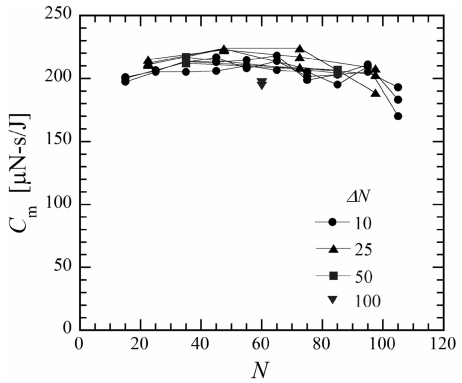

Fig. 13 C_m variations for $\phi = 31.8$ J/cm^2, $P_0 = 10^{-2}$ Pa, $E = 10.9$ J, and $d = 6.6$ mm.

for $\Delta N = 100$. At first C_m increased slightly, but in $30 < N < 60$, it stayed almost constant: $210 \pm 10 \mu$N · s/J. For $N > 60$, C_m started to decrease. As shown in Fig. 14, the depth-to-diameter ratio of the crater at $N = 110$ equaled 1.1 ± 0.1, whereas in the nominal condition (Fig. 10), this ratio was 0.58 ± 0.07. The impulse

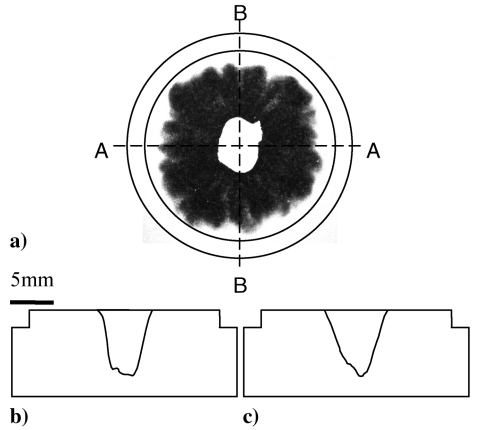

Fig. 14 Sketch of crater: a) front view, b) cross section A–A, and c) cross section B–B; $N = 110$, $E = 10.9$ J, $d = 6.6$ mm ($\phi = 31.8$ J/cm^2), $P_0 = 10^{-2}$ Pa, and $\Delta N = 100$.

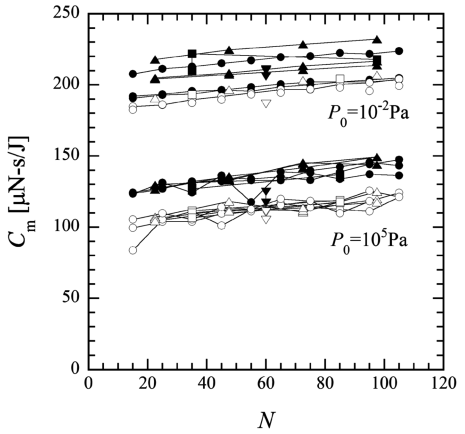

Fig. 15 C_m vs N with $\phi = 19.0 \pm 0.3$ J/cm^2; $d = 8.6$ mm ($E = 10.9$ J) (black symbols), $d = 6.6$ mm ($E = 6.6$ J) (open symbols), $\Delta N = 10$ (circles), $\Delta N = 25$ (upward triangles), $\Delta N = 50$ (squares), and $\Delta N = 100$ (downward triangles).

performance was degraded with the excessive increase in the crater depth.

D. Scaling Effects

Figure 15 shows the impulse characteristics for two spot diameters with an almost constant fluence ($\phi = 19.0 \pm 0.3$). Closed symbols correspond to the data with $d = 8.6$ mm, shown in Fig. 9a, and the open symbols correspond to the smaller spot diameter, $d = 6.6$ mm. C_m for $d = 6.6$ mm was smaller than that for $d = 8.6$ mm by about 5% for $P_0 = 10^{-2}$ Pa and by about 20% for $P_0 = 10^5$ Pa. According to Anju et al. [28], the pressure at the spot center was affected significantly by boundary conditions. The smaller d, the more significant an edge effect becomes and the shorter the period during which expansion waves propagate from the peripheral to the center in the laser spot becomes, whereas the time variation of the laser power was unchanged. Therefore, C_m decreased with decreasing d, with the decrease being larger for the atmospheric pressure. Also, on average, the ablation rate was slightly lower with the smaller d, $\alpha = 140$ μg/J for $d = 6.6$ mm and 150 μg/J for $d = 8.6$ mm, irrespective of the value of P_0.

E. Propulsion Performance

Let us evaluate the aforementioned impulse from the viewpoint of propulsion performance. Let us define the energy conversion efficiency η and the specific impulse I_{sp}, respectively, by

$$\eta \equiv \frac{I_m^2}{2E\Delta m} \tag{13}$$

$$I_{sp} \equiv \frac{I_m}{g\Delta m} \tag{14}$$

where η is equivalent to the thrust efficiency that is used in electric propulsion. From Eqs. (10), (13), and (14), C_m is expressed as a function of these parameters, such that

$$C_m = \frac{I_m}{E} = \frac{2\eta}{gI_{sp}} \tag{15}$$

Figure 16 shows the experimentally measured propulsion performance in the present study. For $P_0 = 10^{-2}$ Pa, $C_m = 200$ μN · s/J, and $\eta = 13\%$ was obtained at $I_{sp} = 130$ s. The present η level is comparable with that of the pulsed plasma thrusters reported in the review paper authored by Burton and Turchi [31] (Table 1). Because in the present experiment the POM target acted as a volume absorber [6], the mass consumption rate (140–150 μg/J) was much higher than those of the pulsed plasma thrusters, 1.5 to 10 μg/J; the propulsion performance obtained in this study was mapped in lower-I_{sp} and higher-C_m regimes. In this

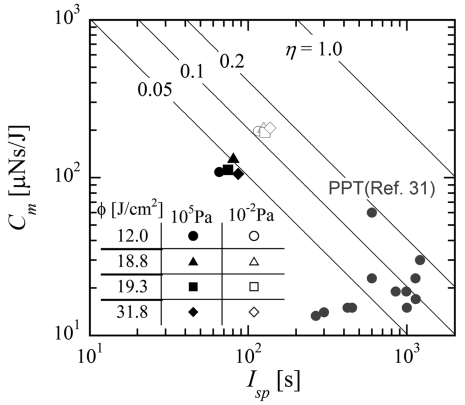

Fig. 16 Propulsion performance under the conditions of Fig. 15; $P_0 = 10^5$ Pa (black symbols), and $P_0 = 10^{-2}$ Pa (open symbols); PPT is the pulsed plasma thruster [31] (gray symbols).

study, the operation fluence range was set based on C_m performance. The examination of the propulsion performance in the higher-I_{sp} regime warrants further investigations to examine various ablation materials, fluence, and laser oscillator specifications.

IV. Conclusions

In this study, we investigated the impulse performance when repetitively irradiating TEA CO_2 laser pulses onto a fixed spot on a POM target. As was reported in the previous studies, a higher momentum coupling coefficient (200 μN · s/J at $I_{sp} = 130$ s, which corresponded to $\eta = 13\%$) was obtained under the reduced ambient pressure of 10^{-2} Pa. The morphology and possible contamination of the virgin target surface degraded the impulse performance. The momentum coupling coefficient was almost constant with respect to the number of laser pulses, yet secondary effects associated with crater formation were observed. For the modest number of laser pulses onto a fixed spot, the impulse performance can be enhanced, apparently due to the aerodynamic expansion owing to the crater formation. With the high fluence, the speed of crater formation became higher; when the eccentricity of the crater became excessively large, C_m decreased. This suggests that if the crater shape can be trimmed adequately, high impulse performance can be maintained for an even larger number of laser pulses, the validation of which is the scope of extended studies.

Acknowledgments

This research was supported by the "Ground-Based Research Program for Space Utilization" promoted by the Japan Space Forum

and by Grant-in-Aid no. 19206089 from the Japan Ministry of Education, Culture, Sports, Science and Technology. The authors cordially appreciate valuable technical support from Andreas Staeb (a special research student from Stuttgart University), T. Ogawa (Technical Division, Institute of Fluid Science, Tohoku University), and A. Saito (Technical Division, School of Engineering, Nagoya University).

References

[1] Kantrowitz, A., "Propulsion to Orbit by Ground-Based Lasers," *Astronautics and Aeronautics*, Vol. 10, No. 5, 1972, pp. 74–76.

[2] Knecht, S. D., Larson, C. W., and Mead, F. B., "Comparison of Ablation Performance in Laser Lightcraft and Standardized Mini-Thruster," *Beamed Energy Propulsion*, edited by K. Komurasaki, T. Yabe, S. Ucnida, and A. Sasoh, Vol. 830, American Inst. of Physics, Melville, NY, 2006, pp. 615–627.

[3] Schall, W. O., Eckel, H. A., Mayerhofer, W., Riede, W., and Zeyfang, E., "Comparative Lightcraft Impulse Measurement," *Proceedings of High-Power Laser Ablation 4*, Vol. 4760, The International Society for Optical Engineering, Bellingham, 2002, pp. 908–917.

[4] Gregg, D. W., and Thomas, S. J., "Momentum Transfer Produced by Focused Laser Giant Pulses," *Journal of Applied Physics*, Vol. 37, No. 7, 1966, pp. 2787–2789.
doi:10.1063/1.1782123

[5] Phipps, C., Turner, T. P., Harrison, R. F., York, G. W., Osborne, W. Z., Anderson, G. K., Colris, X. F., Haynes, L. C., Steele, H. S., Spicochi, K. C., and King, T. R., "Impulse Coupling to Targets in Vacuum by KrF, HF, and CO_2 Single-Pulse Lasers," *Journal of Applied Physics*, Vol. 64, Aug. 1988, pp. 1083–1096.
doi:10.1063/1.341867

[6] Phipps, C., Harrison, R. F., Shimada, T., York, G. W., Turner, T. P., Corlis, X. F., Steele, H. S., and Haynes, L. C., "Enhanced Vacuum Laser-Impulse Coupling by Volume Absorption at Infrared Wavelengths," *Laser and Particle Beams*, Vol. 8, Nos. 1–2, 1990, pp. 281–298.

[7] Phipps, C. R., and Michaelis, M. M., "LISP: Laser Impulse Space Propulsion," *Laser and Particle Beams*, Vol. 12, No. 1, 1994, pp. 23–54.

[8] Pakhomov, A. V., and Gregory, D. A., "Ablative Laser Propulsion: An Old Concept Revisited," *AIAA Journal*, Vol. 38, No. 4, 2000, pp. 725–727.

[9] Pakhomov, A. V., Thompson, M. S., Swift, W., Jr., and Gregory, D. A., "Ablative Laser Propulsion: Specific Impulse and Thrust Derived from Force Measurements," *AIAA Journal*, Vol. 40, No. 11, 2002, pp. 2305–2311.

[10] Pakhomov, A. V., Lin, J., and Tan, R., "Air Pressure Effect on Propulsion with Transeversely Excited Atmospheric CO_2 Laser," *AIAA Journal*, Vol. 44, No. 1, 2006, pp. 136–141.
doi:10.2514/1.11580

[11] Lin, J., Hughes, J., and Pakhomov, A. V., "Experimental study of coupling coefficients for propulsion on TEA CO_2 Laser," *Beamed Energy Propulsion*, Vol. 702, American Inst. of Physics, Melville, NY, 2004, pp. 122–128.

[12] Yabe, T., Phipps, C., Yamaguchi, M., Nakagawa, R., Aoki, K., Mine, H., Ogata, Y., Baasandash, C., Nakagawa, M., Fujiwara, E., Yoshida, K., Nishiguchi, A., and Kajiwara, I., "Microairplane Propelled by Laser Driven Exotic Target," *Applied Physics Letters*, Vol. 80, June 2002, pp. 4318–4320.
doi:10.1063/1.1485313

[13] Watanabe, K., and Sasoh, A., "Impulse Generation Using 300-J Class Laser with Confinement Geometries in Air," *Transactions of the Japan Society for Aeronautical and Space Sciences*, Vol. 48, No. 159, 2005, pp. 49–52.
doi:10.2322/tjsass.48.49

[14] Watanabe, K., Mori, K., and Sasoh, A., "Ambient Pressure Dependence of Laser-Induced Impulse of Polyacetal," *Journal of Propulsion and Power*, Vol. 22, No. 5, 2006, pp. 1150–1153.
doi:10.2514/1.22750

[15] Remo, J. L., "High-Power-Pulsed 1054-Nm Laser-Induced Shock Pressure and Momentum, And Energy Coupling to Iron-Nickel and Stony Meteorites," *Laser and Particle Beams*, Vol. 17, No. 1, 1999, pp. 25–44.
doi:10.1017/S0263034699171039

[16] D'Souza, B. C., and Ketsdever, A. D., "Investigation of Time-Dependent Forces on a Nano-Newton-Second Impulse Balance," *Review of Scientific Instruments*, Vol. 76, 2005, Paper 015105.
doi:10.1063/1.1834707

[17] D'Souza, B. C., and Ketsdever, A. D., "Direct Impulse Measurement of Ablation Processes from Laser-Surface Interactions," AIAA Paper 2005-5172, June 2005.

[18] McMordie, J. A., and Roberts, P. D., "The Interaction of Pulsed CO_2 Laser Radiation with Aluminium," *Journal of Physics D: Applied Physics*, Vol. 8, No. 7, 1975, pp. 768–781.
doi:10.1088/0022-3727/8/7/009

[19] Dufresne, D., Bournot, Ph., Caressa, J. P., Bosca, G., and David, J., "Pressure and Impulse on an Aluminium Target from Pulsed Laser Irradiation at Reduced Ambient Pressure," *Applied Physics Letters*, Vol. 38, No. 4, 1981, pp. 234–236.
doi:10.1063/1.92327

[20] Ageev, V. P., Barchukov, A. I., Bunkin, F. V., Konov, V. I., Puzhaev, S. B., Silenok, A. S., and Chapliev, N. I., "Heating of Metals by CO_2 Laser Radiation Pulses," *Soviet Journal of Quantum Electronics*, Vol. 9, No. 1, 1979, pp. 43–47.
doi:10.1070/QE1979v009n01ABEH008568

[21] Mori, K., Anju, K., Sasoh, A., and Zaretsky, E., "Acceleration History in Laser-Ablative Impulse Measured Using Velocity Interferometer (VISAR)," *High-Power Laser Ablation VI*, edited by C. Phipps, Proceedings of SPIE, Vol. 6261, International Society for Optical Engineering, Bellingham, WA, 2006, Paper 626125.

[22] Phipps, C., "ORION, Challenges and Benefits," *High-Power Laser Ablation*, edited by C. Phipps, Proceedings of SPIE, Vol. 3343, International Society for Optical Engineering, Bellingham, WA, 1998, pp. 575–582.

[23] Phipps, C., Luke, J., Lippert, T., Hauer, M., and Wokaun, A., "Micropropulsion Using a Laser Ablation Jet," *Journal of Propulsion and Power*, Vol. 20, No. 6, 2004, pp. 1000–1011.
doi:10.2514/1.2710

[24] Makropoulou, M., Serafetinides, A. A., and Skordoulis, C. D., "Ultra-Violet and Infra-Red Laser Ablation Studies of Biocompatible Polymers," *Lasers in Medical Science*, Vol. 10, No. 3, 1995, pp. 201–206.
doi:10.1007/BF02133332

[25] Brygo, F., Semerok, A., Oltra, R., Weulersse, J.-M., and Fomichev, S., "Laser Heating and Ablation at High Repetition Rate in Thermal Confinement Regime," *Applied Surface Science*, Vol. 252, No. 23, 2006, pp. 8314–8318.
doi:10.1016/j.apsusc.2005.11.036

[26] Davis, G. M., and Gower, M. C., "Time Resolved Transmission Studies of Poly(Methyl Methacrylate) Films During Ultraviolet Laser Ablative Photodecomposition," *Journal of Applied Physics*, Vol. 61, No. 5, 1987, pp. 2090–2092.
doi:10.1063/1.338015

[27] Frerichs, H., Stricker, J., Wesner, D. A., and Kreutz, E. W., "Laser-Induced Surface Modification and Metallization of Polymers," *Applied Surface Science*, Vol. 86, Feb. 1995, pp. 405–410.
doi:10.1016/0169-4332(94)00431-5

[28] Anju, K., Sawada, K., Sasoh, A., Mori, K., and Zaretsky, E., "Time-Resolved Measurements of Impulse Generation in Pulsed Laser-Ablative Propulsion," *Journal of Propulsion and Power*, Vol. 24, No. 2, 2008, pp. 322–329.
doi:10.2514/1.32017

[29] Lugoner, S., and Fukumoto, Y., "Hierarchical Instability of Vortex Ring Array in Multiple Laser-Matter Interactions," *Fluid Dynamics Research*, Vol. 36, Nos. 4–6, 2005, pp. 277–290.
doi:10.1016/j.fluiddyn.2004.06.005

[30] Zheng, Z. Y., Zhang, J., Lu, X., Hao, Z. Q., Yuan, X. H., Wang, Z. H., and Wei, Z. Y., "Characteristic Investigation of Ablative Laser Propulsion Driven by Nanosecond Laser Pulses," *Applied Physics A: Materials Science and Processing*, Vol. 83, No. 2, 2006, pp. 329–332.
doi:10.1007/s00339-006-3498-z

[31] Burton, R. L., and Turchi, P. J., "Pulsed Plasma Thruster," *Journal of Propulsion and Power*, Vol. 14, No. 5, 1998, pp. 716–735.

G. Spanjers
Associate Editor